Biochemical Basis for the Functional Switch That Regulates Hepatocyte Growth Factor Receptor Tyrosine Kinase Activation[†]

Payal R. Sheth,[‡] John L. Hays,[‡,§] Lisa A. Elferink,[‡] and Stanley J. Watowich*[,‡,||]

Department of Biochemistry and Molecular Biology and Sealy Center for Structural Biology and Molecular Biophysics, University of Texas Medical Branch, Galveston, Texas 77555-0645

Received September 14, 2007; Revised Manuscript Received January 21, 2008

ABSTRACT: Ligand-induced dimerization of receptor tyrosine kinases (RTKs) modulates a system of linked biochemical reactions, sharply switching the RTK from a quiescent state to an active state that becomes phosphorylated and triggers intracellular signaling pathways. To improve our understanding of this molecular switch, we developed a quantitative model for hepatocyte growth factor receptor (c-MET) activation using parameters derived in large part from c-MET kinetic and thermodynamic experiments. Our model accurately produces the qualitative and quantitative dynamic features of c-MET phosphorylation observed in cells following ligand binding, including a rapid transient buildup of phosphorylated c-MET at high ligand concentrations. In addition, our model predicts a slow buildup of phosphorylated c-MET under conditions of reduced phosphatase activity and no extracellular agonist. Significantly, this predicted response is observed in cells treated with phosphatase inhibitors, further validating our model. Parameter sensitivity studies clearly show that synergistic oligomerization-dependent changes in c-MET kinetic, thermodynamic, and dephosphorylation properties result in the selective activation of the dimeric receptor, confirming that this model can be used to accurately evaluate the relative importance of linked biochemical reactions important for c-MET activation. Our model suggests that the functional differences observed between c-MET monomers and dimers may have incrementally evolved to optimize cell surface signaling responses.

The observed nonlinearity of intracellular signaling pathways is believed to enable small changes in reaction kinetics or input signals to be highly amplified, generating large changes in the downstream signaling responses necessary for cell proliferation, differentiation, migration, and motility (*1–7*). The amplitude, duration, and strength of many intracellular signaling responses are dependent on the activation of receptor tyrosine kinases (RTKs),[1] where activation is defined as receptor phosphorylation and subsequent downstream signaling. These observations suggest RTK activation is a critical and tightly regulated process under normal physiological conditions (*3, 8, 9*). Although several essential aspects of RTK activation have been defined, the detailed biochemical, structural, and dynamic processes that regulate RTKs and enable them to selectively induce intracellular signaling in response to extracellular ligand binding are poorly understood (*3, 7, 9, 10*).

It is demonstrated that autophosphorylation regulates RTK [e.g., c-MET receptor; epidermal growth factor receptor (EGFR)] catalytic activity and creates binding sites for effector molecule recruitment (*11–15*). Autophosphorylation has been reported to occur more rapidly in ligand-bound oligomeric RTKs [e.g., insulin growth factor receptor (IGFR)] relative to monomeric RTKs (*16, 17*). Thus, the dominant role of ligand-mediated RTK oligomerization is thought to be promotion of autophosphorylation of tyrosine residues within the receptor's activation loop critical for receptor catalytic function. However, recent studies demonstrate that monomeric RTKs can also be rapidly phosphorylated on tyrosine residues involved in intracellular signal propagation (*18–20*), raising the question of exactly how ligand-dependent dimerization regulates RTK activation.

Our work and that of others suggest that ligand-dependent oligomerization may rapidly and selectively switch a RTK between distinct inactive and active states (*16–18, 21–24*), where the active state exists when a RTK is autophosphorylated and capable of binding to and signaling through immediate downstream effector substrates (e.g., PI3K, Shc,

[†] This work was supported by Grant 4952–052 (S.J.W.) from the Texas Higher Education coordinating Board, by the Sealy Center for Structural Biology (University of Texas Medical Branch), by the McLaughlin Foundation (P.R.S.), and in part by Grants CA112605 and CA119075 (L.A.E.) from the National Institutes of Health. J.L.H. was supported in part by a training fellowship from the National Library of Medicine Training Program of the W. M. Keck Center for Interdisciplinary Bioscience Training of the Gulf Coast Consortia.

* To whom correspondence should be addressed: Department of Biochemistry and Molecular Biology, University of Texas Medical Branch, 301 University Blvd., Galveston, TX 77550-0645. Telephone: (409) 747-4749. Fax: (409) 747-4745. E-mail:watowich@xray.utmb.edu.

[‡] Department of Biochemistry and Molecular Biology.

[§] Current address: Department of Internal Medicine, Wake Forest University School of Medicine, Medical Center Boulevard, Winston-Salem, NC 27127.

[||] Sealy Center for Structural Biology and Molecular Biophysics.

[1] Abbreviations: RTK, receptor tyrosine kinase; PTP, protein tyrosine phosphatase; PDGF, platelet-derived growth factor; EGF, epidermal growth factor; HGF, hepatocyte growth factor; IR, insulin receptor; Tyr, tyrosine-containing effector; pTyr, phosphorylated tyrosine-containing effector; InlB, Internalin B; PY, phosphotyrosine; Y, tyrosine.

10.1021/bi701892f CCC: $40.75
Published on Web 03/07/2008

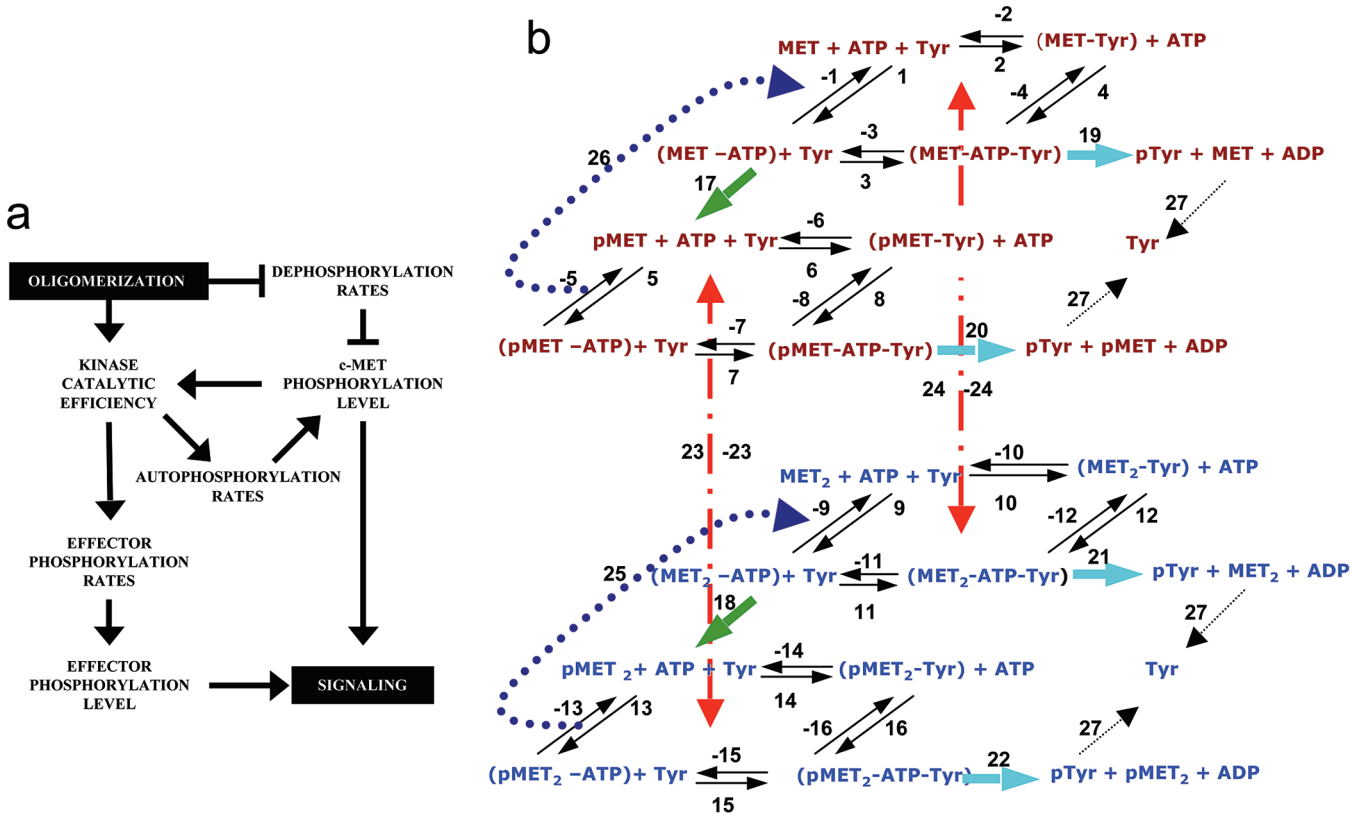

FIGURE 1: c-MET activation model. (a) A feed-forward loop likely regulates c-MET activation. Ligand-induced c-MET oligomerization increases the kinase activity of the receptor, which results in buildup of phosphorylated c-MET by autophosphorylation. Oligomerization reduces c-MET's susceptibility to PTP-catalyzed dephosphorylation, which negatively regulates c-MET phosphorylation. Thus, oligomerization amplifies the buildup of phosphorylated c-MET via a feed-forward loop. The increased kinase catalytic efficiency also increases effector phosphorylation rates, which controls the buildup of activated effector. Phosphorylated c-MET and effector buildup are critical determinants of c-MET activation. (b) Schematic representation of reactions necessary for c-MET activation. The numbering of the reactions was consistent with equations in Tables 1 and 2. Thermodynamic interactions (1–16, solid lines) were described by on/off rates and the concentration of dependent species. The kinetic reactions (17–24, green and blue dashed lines) were described by the catalytic efficiency of the enzyme species for autophosphorylation and effector phosphorylation, respectively, and concentrations of reactants. The extracellular ligand-mediated dimerization process (23 and 24, red dashed line) was described by on/off rate constants and the concentrations of extracellular ligand MET, c-MET monomer (MET), c-MET dimer (MET_2), ATP, and tyrosine-containing effector (Tyr). The prefix p identifies the phosphorylated form of the molecule. Reactions associated with the c-MET monomer and dimer are colored brown and blue, respectively.

Gab1, and Grb2) (*3, 6, 7, 25, 26*). The inactive state exists when a RTK is unphosphorylated and unable to bind to and/or phosphorylate immediate downstream effectors. However, neither functional state is restricted to a particular oligomeric state, consistent with the detection of monomeric active states and oligomeric inactive states (*18–20*).

Activation of the hepatocyte growth factor receptor (c-MET) triggers complex intracellular signaling responses leading to cell proliferation, differentiation, branching morphogenesis, motility, and invasion (*26, 27*). Prolonged c-MET activation correlates closely with tumor progression and metastasis. Previous studies show that MET oligomerization modifies its thermodynamic, kinetic, and catalytic properties (*21, 22*) and that the phosphorylation of the MET activation loop modified its kinase catalytic activity (*15*). In addition, the susceptibility of MET to dephosphorylation is modulated by oligomerization (*20*). These qualitative observations suggest that a feed-forward loop exists among the c-MET phosphorylation state, oligomerization state, and kinase catalytic activity, which effectively amplifies and sharpens the separation between c-MET active and inactive states (Figure 1a). The regulation of this feed-forward loop is accomplished by shifting between the unligated monomeric and ligand-bound dimeric states of c-MET (*26, 28–30*), although the biochemical mechanisms regulating these transitions remain unclear.

In this paper, we present a mathematical description of a feed-forward loop that regulates c-MET activation. This model is described by coupled differential equations that allow time-dependent quantification of all c-MET intermediates and their contribution to c-MET activation that enables the shifts between c-MET inactive and active states to be predicted. This model enables the relative importance of the biochemical reactions that regulate c-MET activation to be clearly measured. An in-depth understanding of c-MET activation could promote development of novel therapeutic approaches to treating c-MET-mediated tumorigenesis and metastasis.

EXPERIMENTAL PROCEDURES

Detailed Mathematical Model. The model describes activation of c-MET by 28 biochemical events that include 15 intermediate species that are central to the activation process of the RTK. Coupled differential equations were used to express the time-dependent concentrations of reaction intermediates and products shown in Figure 1b. These sets of equations provide a mathematical description of the feed-

Table 1: Kinetic Equations Describing the Reaction Pathways Shown in Figure 1B[a]

$d[MET]/dt = \nu_{-1} + \nu_{-2} + \nu_{-24} + \nu_{26} + \nu_{19} - \nu_1 - \nu_2 - \nu_{24}$

$d[ATP]/dt = \nu_{-1} + \nu_{-4} + \nu_{-5} + \nu_{-8} + \nu_{-9} + \nu_{-12} + \nu_{-13} + \nu_{-16} - \nu_1 - \nu_4 - \nu_5 - \nu_8 - \nu_9 - \nu_{12} - \nu_{13} - \nu_{16}$

$d[Tyr]/dt = \nu_{-2} + \nu_{-3} + \nu_{-6} + \nu_{-7} + \nu_{-10} + \nu_{-11} + \nu_{-14} + \nu_{-15} - \nu_2 - \nu_3 - \nu_6 - \nu_7 - \nu_{10} - \nu_{11} - \nu_{14} - \nu_{15}$

$d[MET{-}Tyr]/dt = \nu_2 + \nu_{-4} + \nu_{-24} + \nu_{26} - \nu_{-2} - \nu_4 - \nu_{24}$

$d[MET{-}ATP]/dt = \nu_1 + \nu_{-3} + \nu_{-24} + \nu_{26} - \nu_{-1} - \nu_3 - \nu_{24} - \nu_{17}$

$d[MET{-}ATP{-}Tyr]/dt = \nu_3 + \nu_4 + \nu_{-24} + \nu_{26} - \nu_{-3} - \nu_{-4} - \nu_{24} - \nu_{19}$

$d[pMET]/dt = \nu_{-5} + \nu_{-6} + \nu_{-23} + \nu_{17} - \nu_5 - \nu_6 - \nu_{23} - \nu_{26}$

$d[pMET{-}ATP]/dt = \nu_5 + \nu_{-7} + \nu_{-23} - \nu_{26} - \nu_{-5} - \nu_7 - \nu_{23}$

$d[pMET{-}Tyr]/dt = \nu_6 + \nu_{-8} + \nu_{-23} - \nu_{26} - \nu_{-6} - \nu_8 - \nu_{23}$

$d[pMET{-}ATP{-}Tyr]/dt = \nu_7 + \nu_8 + \nu_{-23} - \nu_{26} - \nu_{-7} - \nu_{-8} - \nu_{24} - \nu_{20}$

$d[MET_2]/dt = \nu_{-9} + \nu_{-10} + \nu_{24} + \nu_{25} - \nu_9 - \nu_{10} - \nu_{24}$

$d[MET_2{-}ATP]/dt = \nu_9 + \nu_{-11} + \nu_{24} + \nu_{25} - \nu_{-9} - \nu_{11} - \nu_{-24} - \nu_{18}$

$d[MET_2{-}Tyr]/dt = \nu_{10} + \nu_{-12} + \nu_{24} + \nu_{25} - \nu_{-10} - \nu_{12} - \nu_{-24}$

$d[MET_2{-}ATP{-}Tyr]/dt = \nu_{11} + \nu_{12} + \nu_{24} + \nu_{25} - \nu_{-11} - \nu_{-12} - \nu_{-24} - \nu_{21}$

$d[pMET_2]/dt = \nu_{-13} + \nu_{-14} + \nu_{23} + \nu_{18} - \nu_{13} - \nu_{14} - \nu_{25} - \nu_{-23}$

$d[pMET_2{-}ATP]/dt = \nu_{13} + \nu_{-15} + \nu_{23} - \nu_{25} - \nu_1 - \nu_2 - \nu_{-23}$

$d[pMET_2{-}Tyr]/dt = \nu_{14} + \nu_{-16} + \nu_{23} - \nu_{25} - \nu_{-14} - \nu_{16} - \nu_{-23}$

$d[pMET_2{-}ATP{-}Tyr]/dt = \nu_{15} + \nu_{16} + \nu_{23} - \nu_{25} - \nu_{-15} - \nu_{-16} - \nu_{-23} - \nu_{22}$

$d[pTyr]/dt = \nu_{19} + \nu_{20} + \nu_{21} + \nu_{22} - \nu_{27}$

[a] Each reaction j in Figure 1b has an associated concentration dependence rate ν_j expression described in Table 2. Reactions 23−27 have identical rate constants but differ in the concentration of their reactants.

forward loop shown in Figure 1a. Given initial conditions, rate constants for the forward and reverse reactions (k_{on} and k_{off}, respectively), catalytic efficiencies for the enzymatic reactions, and the time interval, Mathematica 4.1 was used to solve our set of simultaneous differential equations to give concentrations of any species at any given time point.

This model describes a minimal number of reactions required to generate a downstream signal (Figure 1b). In its simplest form, the c-MET receptor is at the cell surface as a nonsignaling monomer that can bind ATP and a tyrosine-containing effector molecule (Tyr) (reactions 1–4). The abbreviation Tyr, which is used throughout the paper, represents a generic effector substrate that contains a Tyr residue that undergoes phosphorylation. The monomeric, nonphosphorylated receptor either can become autophosphorylated (reaction 17, Figure 1b) or may phosphorylate the Tyr effector (reaction 19, Figure 1b). Similarly, the phosphorylated monomer can bind ATP and Tyr to form a ternary complex (reactions 5–8, Figure 1b). The phosphorylated and nonphosphorylated c-MET may dimerize in response to extracellular ligand binding (reactions 23, –23, 24, and –24, Figure 1b). Also, the phosphorylated receptor can be dephosphorylated (reactions 25 and 26, Figure 1b) by cellular protein tyrosine phosphatases (PTPs). Dephosphorylation of the Tyr effector is included in the model as this down-regulatory reaction is present in cells. Not included in the current model is the formation of multiple phosphorylated c-MET species, although the addition of multiple reactions and catalytic efficiencies can be easily done when experimental data become available for these reactions. The kinetic and thermodynamic parameters are for fully phosphorylated c-MET, as those are the data currently available either from our laboratory or from the literature as described below.

A complete set of the kinetic equations used to describe the activation of the c-MET receptor can be found in Table 1. For example, the concentration of the binary complex ([MET−ATP]) at any given time is equal to the rate of production of the binary complex less its consumption. The production of the binary complex can be described by the rate of formation from free MET and free ATP, the rate of dissociation of the ternary complex ([MET−ATP−Tyr]) into the MET−ATP complex and free Tyr, the rate of monomerization of the MET_2−ATP complex into the MET−ATP complex, and the dephosphorylation of the pMET−ATP complex into the MET−ATP complex. The rate of consumption of the binary MET−ATP complex is equal to the reverse of the reactions mentioned above with the loss due to the kinetic autophosphorylation reaction instead of the dephosphorylation reaction. Mathematically, this can be expressed as

$$d[MET{-}ATP]/dt = \nu_1\nu_{-3}\nu_{-24}\nu_{26}\nu_{-1}\nu_3\nu_{24}\nu_{17}$$

where, ν_x is the rate of reaction x from Figure 1b. The exact values of the rate equations are enumerated in Table 2. In the overall activation process, the receptor concentration is assumed to be conserved such that $[MET]_{total} = [MET]_{free} + [MET] + [MET{-}ATP] + [MET{-}Tyr] + [MET{-}ATP{-}Tyr] + [pMET] + [pMET{-}ATP] + [pMET{-}Tyr] + [pMET{-}ATP{-}Tyr] + [MET_2] + [MET_2{-}ATP] + [MET_2{-}Tyr] + [MET_2{-}ATP{-}Tyr] + [pMET_2] + [pMET_2{-}ATP] + [pMET_2{-}Tyr] + [pMET_2{-}ATP{-}Tyr] = \text{constant}$. The initial response in the computer model easily accounts for this assumption. In cells, c-MET is internalized and degraded through endosomal trafficking, each of which occurs in the time frame of minutes (*31, 32*). Since we focus on initial activation of the receptor which occurs within ~200 s, the contribution of receptor internalization and degradation is assumed to be negligible.

Parameter Values. Our detailed activation model containing the 28 biochemical events described earlier utilizes 48 different parameters (42 rate constants and six Michaelis–Menten constants). As described below, 36 of these 48 parameters are either directly measured or derived from the measured parameters for the c-MET system. This represents a considerable number of accurate c-MET experimental parameters for inclusion in a computational model of this size.

In our model, we use k_{on} and k_{off} values that had been previously determined in our laboratory for reactions 5–8 and 13–16 (*22*). Similarly, the kinetic catalytic efficiencies for reactions 20 and 22 were described by our laboratory (*21*). Although we have not directly measured k_{on} and k_{off} values for the dephosphorylated forms of c-MET, other groups showed that equilibrium dissociation constants between phosphorylated and dephosphorylated RTK catalytic domains differ by a factor of 2 (*11*). Thus, it was reasonable to estimate that the on and off rates for the ATP and effector to the dephosphorylated c-MET were on the same order of magnitude as those of the c-MET-phosphorylated form. This assumption was tested with our model, and order of magnitude changes to on and off rates for substrate binding to dephosphorylated c-MET did not affect the shape of the response curves for the total phosphorylated receptor and pTyr.

Naldini et al. (*33*) assessed the phosphorylation of exogenous substrates by phosphorylated and dephosphorylated c-MET immunoprecipitated from cell lysates and observed

Table 2: Rate Equations Describing the Reaction Pathways Shown in Figure 1B[a]

$\nu_1 = k_1[\text{MET}][\text{ATP}]$; $k_1 = 0.01$
$\nu_2 = k_2[\text{MET}][\text{Tyr}]$; $k_2 = 0.001$
$\nu_3 = k_3[\text{MET}-\text{ATP}][\text{Tyr}]$; $k_3 = 0.001$
$\nu_4 = k_4[\text{MET}-\text{Tyr}][\text{ATP}]$; $k_4 = 0.01$
$\nu_5 = k_5[\text{pMET}][\text{ATP}]$; $k_5 = 0.1$
$\nu_6 = k_6[\text{pMET}][\text{Tyr}]$; $k_6 = 0.00032$
$\nu_7 = k_7[\text{pMET}-\text{ATP}][\text{Tyr}]$; $k_7 = 0.0015$
$\nu_8 = k_8[\text{pMET}-\text{Tyr}][\text{ATP}]$; $k_8 = 0.1$
$\nu_9 = k_9[\text{MET}_2][\text{ATP}]$; $k_9 = 0.01$
$\nu_{10} = k_{10}[\text{MET}_2][\text{Tyr}]$; $k_{10} = 0.001$
$\nu_{11} = k_{11}[\text{MET}_2-\text{ATP}][\text{Tyr}]$; $k_{11} = 0.001$
$\nu_{12} = k_{12}[\text{MET}_2-\text{Tyr}][\text{ATP}]$; $k_{12} = 0.01$
$\nu_{13} = k_{13}[\text{pMET}_2][\text{ATP}]$; $k_{13} = 0.1$
$\nu_{14} = k_{14}[\text{pMET}_2][\text{Tyr}]$; $k_{14} = 0.001$
$\nu_{15} = k_{15}[\text{pMET}_2-\text{ATP}][\text{Tyr}]$; $k_{15} = 0.001$
$\nu_{16} = k_{16}[\text{pMET}_2-\text{Tyr}][\text{ATP}]$; $k_{16} = 0.1$
$\nu_{17} = k_{17}[\text{MET}-\text{ATP}]$; $k_{17} = 0.0008$
$\nu_{18} = k_{18}[\text{MET}_2-\text{ATP}]$; $k_{18} = 0.24$
$\nu_{19} = k_{19}[\text{MET}-\text{ATP}-\text{Tyr}]$; $k_{19} = 0.0008$
$\nu_{20} = k_{20}[\text{pMET}-\text{ATP}-\text{Tyr}]$; $k_{20} = 0.008$
$\nu_{21} = k_{21}[\text{MET}_2-\text{ATP}-\text{Tyr}]$; $k_{21} = 0.0024$
$\nu_{22} = k_{22}[\text{pMET}_2-\text{ATP}-\text{Tyr}]$; $k_{22} = 0.024$
$\nu_{23} = k_{23}[\text{MET}][\text{GF}]$; $k_{23} = 10$
$\nu_{24} = k_{24}[\text{pMET}][\text{GF}]$; $k_{24} = 10$
$\nu_{25} = (V_{25}[\text{pMET}_2])/(K_{25} + [\text{pMET}_2])$; $V_{25} = 0.045$, $K_{25} = 0.01$
$\nu_{26} = (V_{26}[\text{pMET}])/(K_{26} + [\text{pMET}])$; $V_{26} = 0.45$, $K_{26} = 0.01$
$\nu_{27} = (V_{27}[\text{pTyr}])/(K_{27} + [\text{pTyr}])$; $V_{27} = 0.001$, $K_{27} = 0.1$

$\nu_{-1} = k_{-1}[\text{MET}-\text{ATP}]$; $k_{-1} = 0.34$
$\nu_{-2} = k_{-2}[\text{MET}-\text{Tyr}]$; $k_{-2} = 0.3$
$\nu_{-3} = k_{-3}[\text{MET}-\text{ATP}-\text{Tyr}]$; $k_{-3} = 0.18$
$\nu_{-4} = k_{-4}[\text{MET}-\text{ATP}-\text{Tyr}]$; $k_{-4} = 0.29$
$\nu_{-5} = k_{-5}[\text{pMET}-\text{ATP}]$; $k_{-5} = 1.7$
$\nu_{-6} = k_{-6}[\text{pMET}-\text{Tyr}]$; $k_{-6} = 0.045$
$\nu_{-7} = k_{-7}[\text{pMET}-\text{ATP}-\text{Tyr}]$; $k_{-7} = 0.10$
$\nu_{-8} = k_{-8}[\text{pMET}-\text{ATP}-\text{Tyr}]$; $k_{-8} = 1.43$
$\nu_{-9} = k_{-9}[\text{MET}_2-\text{ATP}]$; $k_{-9} = 0.114$
$\nu_{-10} = k_{-10}[\text{MET}_2-\text{Tyr}]$; $k_{-10} = 0.024$
$\nu_{-11} = k_{-11}[\text{MET}_2-\text{ATP}-\text{Tyr}]$; $k_{-11} = 0.018$
$\nu_{-12} = k_{-12}[\text{MET}_2-\text{ATP}-\text{Tyr}]$; $k_{-12} = 0.166$
$\nu_{-13} = k_{-13}[\text{pMET}_2-\text{ATP}]$; $k_{-13} = 0.57$
$\nu_{-14} = k_{-14}[\text{pMET}_2-\text{Tyr}]$; $k_{-14} = 0.013$
$\nu_{-15} = k_{-15}[\text{pMET}_2-\text{ATP}-\text{Tyr}]$; $k_{-15} = 0.016$
$\nu_{-16} = k_{-16}[\text{pMET}_2-\text{ATP}-\text{Tyr}]$; $k_{-16} = 0.87$
$\nu_{-23} = k_{-23}[\text{MET}_2]$; $k_{-23} = 0.01$
$\nu_{-24} = k_{-24}[\text{pMET}_2]$; $k_{-24} = 0.01$

[a] All rate constants (k) are given in s^{-1} (first-order) and in μM^{-1} s^{-1} (second-order). All catalytic efficiencies (V) are given in μM s^{-1}, and Michaelis–Menten constants (K, reactions 25–27) are in μM. Constants were obtained as described in Experimental Procedures. For reactions 23, −23, 24, and −24, only one example is given, although the dimerization could occur between any two matching species.

the phosphorylated receptor had ~10-fold higher kinase activity than the dephosphorylated receptor. Our kinetic constants for phosphorylated active dimeric TPR−MET were similar to the values obtained by Naldini et al. (*33*) for the phosphorylated immunoprecipitated c-MET. Therefore, we assumed a 10-fold difference in catalytic efficiencies for the dephosphorylated c-MET to phosphorylate exogenous tyrosine substrates compared to phosphorylated c-MET (reactions 19 and 21 vs reactions 20 and 22). Similarly, the ability of unstimulated c-MET to undergo autophosphorylation was assumed to mimic the monomer's ability to phosphorylate exogenous effectors. Therefore, reactions 17 and 19 were assumed to have similar catalytic rates.

Although the mechanism of c-MET autophosphorylation is unknown, evidence of both intermolecular and intramolecular phosphorylation exists for different RTKs (*10, 34–41*). As a starting point for our model, monomer autophosphorylation was assumed to be an intramolecular reaction. Preliminary computation analyses using the autophosphorylation k_{cat} assigned to monomeric c-MET and a *trans* mode of autophosphorylation predicted similar levels of c-MET phosphorylation (data not shown). The catalytic efficiency of dephosphorylated dimeric c-MET is unknown. Since extracellular ligand stimulation induces an ~10-fold increase in the autophosphorylation catalytic activity of the IR (*42*), the activity of reaction 18 was similarly increased relative to that of reaction 22.

Dephosphorylation rate constants for Shc and EGFR were used to approximate the dephosphorylation rates of exogenous effectors (Tyr) and c-MET (*1*). Shc is phosphorylated by c-MET when the receptor is activated by HGF (*43, 44*). It is a well-characterized substrate for c-MET and has been exhaustively studied in the context of c-MET signaling (*44*). Shimizu et al. (*24*) describe an ~10-fold increase in the sensitivity of monomeric versus dimeric PDGFR toward dephosphorylation by recombinant phosphatases. Our studies measured a 10-fold decreased substrate specificity of recombinant PTPβ for phosphorylated dimeric TPR−MET as compared to phosphorylated monomeric cytoMET (*20*). We include a 10-fold difference in V_{max} between the two c-MET dephosphorylation reactions while keeping the K_m equal.

The number of c-MET molecules on the cell surface is unknown. However, in the EGFR system, there are multiple studies that measure ~1–3 × 10^5 molecules/cell, which translates into effective cellular EGFR concentrations within the range of 20–100 nM (*1*). We assumed c-MET and EGFR concentrations to be similar and estimated the c-MET concentration to be 100 nM for our model. The effect of c-MET concentration on the signaling output was simulated using this model. Increases in c-MET concentration have a linear impact on the signaling output, implying c-MET concentration does not play an important role in the synergy highlighted in the paper. The concentrations of tyrosine-containing effector molecules (Tyr) that were phosphorylated by c-MET were taken from previously published results to be 150 nM (*1*). The ATP concentration was assumed to be 1 mM, which was seen to be saturating for this system (*45*). Concentrations of c-MET and Tyr were assumed to be constant throughout the early time points investigated in our model. The ternary complexes of c-MET, ATP, and tyrosine-containing substrate or effector (Tyr) were assumed to be the necessary intermediate complex leading to effector phosphorylation. The mechanistic details of this phosphorylation reaction do not change the time-dependent buildup of phosphorylated c-MET and pTyr. All enzymatic reactions were assumed be irreversible, and PTPs were assumed to follow Michealis−Menten kinetics. The activation model used first-order mass-action kinetics and sets of differential equations described by specific kinetic and thermodynamic parameters.

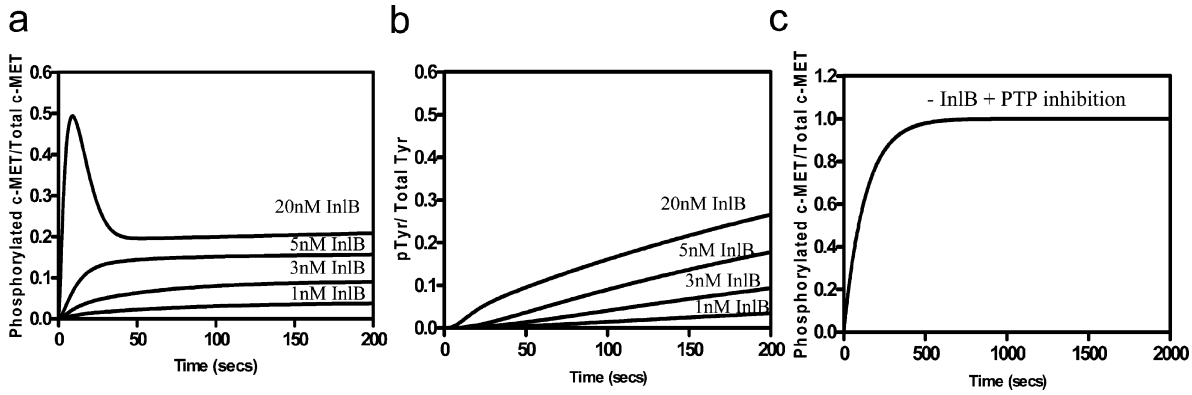

FIGURE 2: Model predictions. (a) Predicted kinetics of c-MET phosphorylation in presence of 1, 3, 5, and 20 nM InlB. (b) Predicted kinetics of effector phosphorylation (pTyr) in the presence 1, 3, 5, and 20 nM InlB. The *y*-axis on the graphs represents the fraction of total c-MET and Tyr-containing effector phosphorylated. (c) Model prediction of the fraction of c-MET phosphorylated as a result of blocking PTP activity associated with monomeric c-MET and no InlB stimulation.

Internalin B (InlB) was used as the extracellular ligand to activate c-MET in computer simulations and corresponding cell culture experiments. InlB was recently identified as a bacterial agonist for c-MET RTK and was shown to mimic c-MET activation and endocytosis following stimulation with a cognate HGF ligand (*32, 46, 47*). Furthermore, InlB initiated c-MET signaling as measured by phosphorylation of Gab1, Cbl, and Shc, along with activation of the PI3K pathway (*48*). K_d values for InlB binding to the extracellular domain of c-MET are in the nanomolar range (*49*). On and off rates for InlB−Met binding, which were more crucial for developing time-dependent models, are unknown. Thus, we use InlB on and off rates consistent with the equilibrium binding constant and the time constraints of the signaling process (*50*). With a k_{on} of 10 μM^{-1} s^{-1} and a k_{off} of 0.01 s^{-1}, the receptor reached a steady-state value within 2 min. Increasing or decreasing the on and off rates by a factor of 10 did not significantly affect the response curves that described buildup of phosphorylated c-MET or pTyr.

Experimental Validation of the c-MET Activation Model. The quantitative and qualitative predictions of the activation model were tested experimentally. The Vero cells (ATCC) used for these studies endogenously expressed c-MET. Prior to any stimulation with extracellular ligand, the cells were grown to ~60% confluency and serum-starved for 12–24 h. For ligand stimulation experiments, cells were stimulated with 1, 5, and 20 nM InlB. At 0, 15, 60, 120, and 300 s post-InlB stimulation, the cells were washed twice with ice-cold PBS for 3 min and subsequently lysed in Triton X-100 lysis buffer [50 mM Tris (pH 7.5), 150 mM NaCl, 1% Triton X-100, 3 mM Na_3VO_4, 2 mM EDTA, 2 mM NaF, and protease inhibitor cocktail]. Protein concentrations in the lysates were determined using a Bio-Rad DC Assay, and 500–1000 μg of total protein was used for c-MET immunoprecipitation with the primary antibody to the c-MET extracellular region (antibody DO-24). Quantitative analyses to determine the percentage of total receptor that was phosphorylated used the strategy described by Kholodenko et al. (*1*). Briefly, cell lysates at each time point were divided into equal parts for parallel immunoprecipitation with the anti-phosphotyrosine (PY)−agarose conjugate and anti-MET (Upstate). The anti-PY immunoprecipitates and the c-MET immunoprecipitates at indicated time points post-ligand stimulation were run on the same gel for immunoblotting with anti-MET antibody (Figure 3a, left panel). InlB-induced c-MET phosphorylation was assessed at early time points when internalization is negligible (*32*). Immunoprecipitation was performed according to standard protocols. Briefly, lysates were incubated with the primary antibody overnight at 4 °C and then incubated with 100 μL of protein A agarose in PBS for 3–4 h at 4 °C to capture the immune complex. The tubes were spun, and beads were washed three or four times in lysis buffer and then resuspended in SDS−PAGE buffer. Samples were separated with 7.5% polyacrylamide gels and SDS−PAGE for subsequent immunoblotting. After an overnight incubation in blocking buffer (1% BSA in TBST) at 4 °C, the membranes were incubated with anti-MET antibody (typically at a 1:1000 dilution) for 1 h at room temperature. After three successive washes in TBST, the membranes were incubated with secondary antibody (1:10000 dilution) for 45 min. The proteins were visualized with an ECL Plus chemiluminescent kit (Amersham) and exposure to film (Kodak X-OMAT AR) (Figure 3a, left panel). The fraction of total c-MET phosphorylated (Figure 3a) in Vero cells was determined from the quantified blots as the ratio of signal from the anti-MET antibody in precipitates from the anti-PY antibody to that from the anti-MET antibody for each time point (*1*). X-ray films containing the protein bands were imaged in a MultiImage Light Cabinet (Alpha Innotech Corp.), and densitometry was performed using ChemiImager provided by the manufacturer. Experiments were performed within the dynamic range of the antibody signal and the exposure time.

The pervanadate stimulation experiments have been previously described (*20*), and quantitative data for these experiments are presented (Figure 3b). Briefly, cells were stimulated with the addition of pervanadate-containing media. At specific time points poststimulation, the cells were lysed and subjected to immunoprecipitation with the anti-MET antibody. The precipitated proteins were separated on denaturing polyacrylamide gels and transferred to a PVDF membrane using protocols outlined above. The membranes were probed with the anti-PY antibody and reprobed with the anti-MET antibody (Figure 3b). Quantitative analyses were used to obtain the fraction of c-MET phosphorylated. At PY signal saturation, it was assumed that all active c-MET receptors were fully phosphorylated. In that case, the fraction of phosphorylated receptor would be the ratio of signal at any time point to the signal measured at saturation.

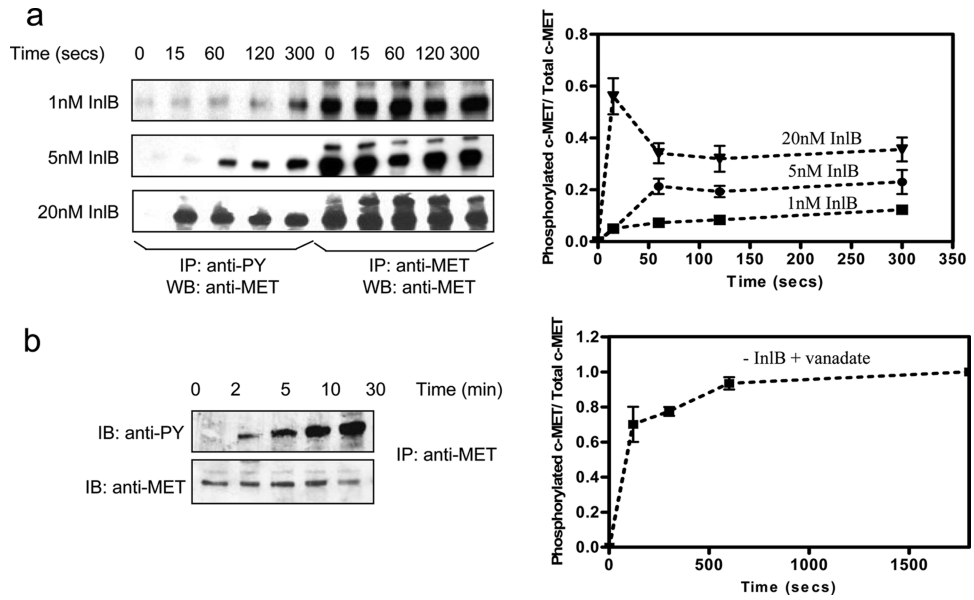

FIGURE 3: Experimental validation of the c-MET activation model. (a) Measured kinetics of c-MET phosphorylation in cultured Vero cells upon stimulation with 1, 5, and 20 nM InlB. (b) Quantitative analyses of c-MET phosphorylation kinetics in the presence of a known PTP inhibitor pervanadate and in the absence of InlB. The data are presented as means of three different experiments with error bars representing the standard error. The representative immunoblots for panels a and b are shown to the left of their respective graphs.

RESULTS

Development of the Kinetic Model. To quantitatively study c-MET activation, a detailed mathematical model was developed that incorporated 28 major biochemical reaction events associated with c-MET dimerization and signaling (Figure 1). As detailed in Experimental Procedures, ~75% of the parameter values in this model are from published kinetic and thermodynamic parameters for monomeric cytoMET and the dimeric TPR−MET complex (*20–22*). The few rate constants in our model that were not available from the c-MET system were derived from experimental data in related RTKs (*1, 5, 16, 24, 33*). Protein–protein interactions were described by mass action equations. Rate equations used for generating our c-MET activation model are listed in Table 2. Starting concentrations of c-MET and Tyr-containing effectors were taken from published results (*1*). The ATP concentration was set at 1 mM (*45*), although the model predictions do not change with higher ATP concentrations (data not shown). Activation of c-MET occurs in response to binding the physiological ligand HGF or the Internalin B (InlB) protein of *Listeria monocytogenes*. InlB has been shown to mimic many of the features of HGF-induced c-MET activation, endocytosis (*32, 46, 47*), and signaling that are relevant for this study (*48*). Accordingly, InlB was used as the c-MET agonist for the simulations and cell culture studies.

c-MET Phosphorylation in the Absence of Agonist. We determined the population distribution of different c-MET species in the absence of an extracellular ligand. With no external ligand stimulus, our model predicts that c-MET would exist predominantly as an ATP-bound unphosphorylated monomeric receptor (denoted MET−ATP in Figure 1b). Since the c-MET monomer has kinase activity (*20–23*), we tested whether significant levels of phosphorylated c-MET monomers can accumulate in the absence of an extracellular ligand. Our model predicts that in the absence of an extracellular ligand the steady-state concentration of phosphorylated c-MET monomers (defined as [pMET] + [pMET−ATP] + [pMET−Tyr] + [pMET−ATP−Tyr]) would be <1% of the total c-MET concentration in cells (data not shown). We could not detect c-MET phosphorylation in unstimulated serum-starved Vero cells using immunoblotting (data not shown). This is likely due to the predicted levels of c-Met being below the level of detection, since small amounts of EGFR basal phosphorylation in unstimulated cells have been reported using a more sensitive FRET-based detection system (*51*). Significantly, this level of monomeric phosphorylated receptor is approximately 2 orders of magnitude smaller than the steady-state levels of phosphorylated dimeric receptor generated in response to added extracellular ligand (Figure 2a).

The basal level of c-MET phosphorylation in the absence of extracellular ligand stimulation directly correlates with changes to the modeled c-MET monomer autophosphorylation (reaction 17, Figure 1b) and dephosphorylation (reaction 26, Figure 1b) rates. Therefore, we examined the impact of setting the c-MET monomer dephosphorylation rate (reaction 26, Figure 1b) to zero. In this extreme case, our model predicts a relatively slow yet substantial buildup of phosphorylated c-MET (Figure 2c). This prediction has been reported in previous cell culture studies, where the buildup of phosphorylated PDGFR (*18*), IR (*19*), and c-MET (*20*) was observed in the presence of phosphatase inhibitors. Our experimental data on c-MET phosphorylation kinetics in the presence of the PTP inhibitor pervanadate (Figure 3b) correlate qualitatively and quantitatively with our model's prediction (Figure 2c). Moreover, our model predicts that the rate of phosphorylated monomeric c-MET accumulation upon inhibition of receptor dephosphorylation is directly related to the c-MET autophosphorylation k_{cat} (reaction 17, Figure 1b). Thus, our model clearly shows c-MET phosphorylation and dephosphorylation processes are likely balanced, resulting in a dynamic steady state.

c-MET Phosphorylation in the Presence of an Extracellular Ligand. Using our c-MET activation model (Figure 1), we calculated the rate and magnitude of c-MET autophos-

phorylation and exogenous effector phosphorylation in response to an extracellular ligand (Figure 2a,b). Our model predicted that the concentration of total phosphorylated c-MET (defined as [pMET] + [pMET−Tyr] + [pMET−ATP] + [pMET−ATP−Tyr] + [$pMET_2$] + [$pMET_2$−Tyr] + [$pMET_2$−ATP] + [$pMET_2$−ATP−Tyr]) was not linearly related to the concentration of added extracellular ligand (Figure 2a). At low InlB concentrations (<5 nM), our model predicted that the phosphorylation of c-MET would reach a maximum steady-state level within seconds (Figure 2a). In contrast, our model predicted that c-MET phosphorylation kinetics at higher InlB concentrations (>5 nM) would produce a rapid transient spike response followed by a steady-state phosphorylation level that was lower than the maximum observed during the transient spike (Figure 2a). The magnitude of the phosphorylated c-MET transient spike and steady-state levels were dependent on the concentration of added extracellular ligand.

We validated our simulations using Vero cells as a model cell culture system (Figure 3a). Vero cells have been extensively used to characterize c-MET signaling following activation with HGF and InlB (*46, 52*). Predictions of c-MET phosphorylation were compared to c-MET phosphorylation levels measured in cultured Vero cells in response to different amounts of InlB (1, 5, and 20 nM). We observe a ligand-dependent nonlinear increase in the level of c-MET phosphorylation in serum-starved Vero cells. In addition, a rapid transient spike in the level of phosphorylated c-MET is observed at 20 nM InlB. Our measured c-MET phosphorylation responses (Figure 3a) correlate closely to our model predictions (Figure 2a), implying our c-MET activation model is sufficient to accurately reproduce the salient features of c-MET activation. Unlike earlier modeling studies (*1*), our activation model does not require the effector-bound state of the receptor to be "inaccessible" to cellular phosphatases to simulate the transient spike in receptor phosphorylation. Instead, the observed transient spike in the level of the phosphorylated receptor following stimulation with high ligand concentrations results from rapid c-MET autophosphorylation prior to cellular phosphatases reaching full activity. In addition, our model interprets the observed steady-state receptor phosphorylation levels as a result of the balance between kinase and phosphatase kinetic reactions once a quasi-equilibrium state is reached. As discussed below, varying parameters associated with dimeric c-MET autophosphorylation (reaction 18, Figure 1b) and dephosphorylation (reaction 25, Figure 1b) reactions significantly modulate the shape and height of the phosphorylated c-MET transient spike in response to ligand stimulation. Our simulations accurately reproduce all tested cell culture observations, validating the applicability of our activation model in improving our understanding of the dynamic processes that regulate c-MET activation.

Computational Analysis of Effector Binding and Phosphorylation. Signaling from activated c-MET requires effectors to bind to c-MET phosphotyrosines, resulting in effector protein phosphorylation and/or activation (*26*). Binding, phosphorylation, and dephosphorylation reactions for c-MET kinase substrates were included in our model. Although multiple effectors may interact with phosphorylated c-MET simultaneously, as a first approximation only one effector is included in our c-MET activation model. Additional complexities associated with multiple-effector binding will be subsequently included in our model once the relevant experimental data are available. The time course for the buildup of the phosphorylated effector (pTyr) is simulated for a range of added extracellular ligand concentrations (Figure 2b). At each extracellular ligand concentration, our c-MET activation model shows that pTyr levels will increase monotonically in response to ligand-induced dimerization; no transient spike is observed in pTyr levels. This pattern of effector phosphorylation was observed for Shc in the related EGFR RTK system (*1*). In addition, our model predicted pTyr accumulated only after significant c-MET phosphorylation, resulting in a lag time between extracellular ligand stimulation and effector phosphorylation (Figure 2). The rate of effector phosphorylation is biphasic (most clearly observed at high extracellular ligand concentrations), with a higher initial rate of effector phosphorylation followed by a slower rate of phosphorylation as the dynamic system reaches steady state (Figure 2b). Finally, the amount of Tyr bound to the c-MET (defined as [MET−Tyr] + [MET−ATP−Tyr] + [pMET−Tyr] + [pMET−ATP−Tyr] + [MET_2−Tyr] + [MET_2−ATP−Tyr] + [$pMET_2$−Tyr] + [$pMET_2$−ATP−Tyr]) correlates closely with the accumulation of phosphorylated c-MET (data not shown). These observations imply that c-MET phosphorylation is necessary for effective effector recruitment and/or phosphorylation, consistent with previous reports that mutants deficient in kinase activity did not result in effector activation in response to InlB or HGF.

Sensitivity of c-MET Signaling to Biochemical Parameters. c-MET activation, described by the magnitude and specificity of c-MET and effector phosphorylation in response to extracellular ligand-mediated dimerization, is controlled by a variety of thermodynamic and kinetic parameters. The sensitivity of dimeric c-MET and effector phosphorylation to these different biochemical parameters was studied in an effort to understand their relative importance in c-MET activation. Sensitivity analysis of c-MET phosphorylation to kinase ATP and effector binding on and off rates reveals that these parameters have little impact on the behavior of the c-MET activation model (data not shown). In contrast, changing the kinetic parameters associated with dimeric c-MET phosphorylation and dephosphorylation reactions has a significant impact on c-MET activation as measured by the level of accumulation of phosphorylated dimeric c-MET and pTyr.

We systematically varied the kinetic parameters associated with dimeric c-MET autophosphorylation (k_{18}), dephosphorylation (V_{25}), and effector phosphorylation (k_{21} and k_{22}) reactions to deepen our understanding of the relative importance of these processes to c-MET activation. Panels a and b of Figure 4 show the time-dependent accumulation of phosphorylated c-MET and pTyr as a function of dimer autophosphorylation k_{cat} (k_{18}) at a saturating (i.e., 20 nM) extracellular ligand concentration. Clearly, the predicted rates of c-MET phosphorylation and steady-state levels of phosphorylated c-MET are dependent on c-MET dimer autophosphorylation values. Furthermore, by affecting the level of phosphorylated c-MET, the autophosphorylation k_{cat} significantly changes the rate of pTyr production (Figure 4b). Thus, the c-MET activation response is sensitive to the dimer autophosphorylation rate. In contrast, changes to the effector

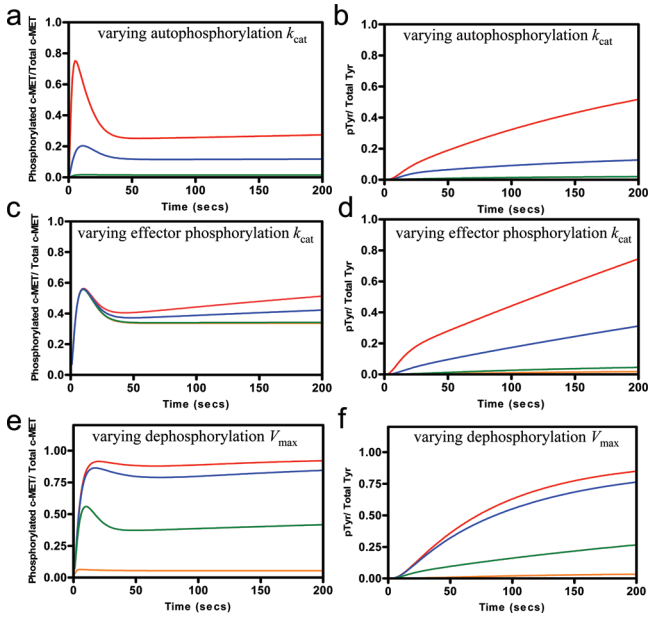

FIGURE 4: Sensitivity of c-MET and Tyr phosphorylation kinetics to the autophosphorylation, effector phosphorylation, and PTP-catalyzed dephosphorylation. (a and b) Predicted kinetics of c-MET (a) and Tyr (b) phosphorylation were calculated using kinase autophosphorylation k_{cat} values of 0.0008 (orange), 0.008 (green), 0.08 (blue), and 0.8 s^{-1} (red). (c and d) Predicted kinetics of c-MET (c) and pTyr (d) phosphorylation at kinase effector phosphorylation k_{cat} values of 0.00024 (orange), 0.0024 (green), 0.024 (blue), and 0.05 s^{-1} (red). (e and f) Predicted kinetics of c-MET (e) and pTyr (f) phosphorylation at dephosphorylation V_{max} values of 0.00045 (red), 0.0045 (blue), 0.045 (green), and 0.45 μM s^{-1} (orange). These simulations were performed using a saturating InlB concentration of 20 nM, conditions under which all the c-MET species are dimeric.

phosphorylation k_{cat} (k_{21} and k_{22}) have little effect on the rate of buildup of phosphorylated c-MET (Figure 4c). However, the rate of pTyr buildup is directly dependent upon the magnitude of the effector phosphorylation k_{cat} (Figure 4d). Phosphorylated c-MET steady-state levels and the rate of pTyr formation are significantly changed when the c-MET dephosphorylation V_{max} (V_{25}) is varied, implying a critical role for cellular phosphatases in modulating c-MET signaling potential (Figure 4e,f). Changes to the steady-state level of phosphorylated c-MET modify the sharpness of the phosphorylated c-MET transient spike observed at high extracellular ligand concentrations (Figure 4e). Thus, the phosphatase-catalyzed dephosphorylation rates dictate the amplitude as well as the duration of c-MET activation.

The simulations described above evaluated the relative importance of kinetic and thermodynamic parameters associated with dimeric c-MET, the predominant activated species. A similar parameter sensitivity analysis was applied to monomeric (i.e., unstimulated) c-MET. In this case, no significant differences are observed in the buildup of phosphorylated c-MET or pTyr when single thermodynamic or kinetic parameters are varied (k_{17}, k_{19}, k_{20}, and k_{26}) (data not shown). In contrast, as discussed in greater detail below, significant changes in the buildup of phosphorylated c-MET and pTyr are observed when several kinetic parameters for monomeric c-MET are simultaneously changed. On the basis of these results, it can be inferred that dimerization is a reversible mechanism for simultaneously adjusting several c-MET kinetic parameters to form the active signaling state.

Table 3: Synergistic Changes to the c-MET Biochemical Properties Were Required for Efficient and Specific c-MET Activation

Model Prediction Levels of pMET and pTyr 100 s Post-InlB Stimulation[a]

[InlB] (nM)	pMET	pTyr
0	1	1
1	127	59
3	278	155
20	566	421

Effect of Incremental Changes in the Kinetic Parameters Associated with Monomeric Species on Steady-State Levels of Phosphorylated c-MET and Effector[b]

[InlB] (nM)	k_{17}	$k_{19,20}$	V_{26}	pMET	pTyr
0	1	1	1	1	1
0	10	1	1	13	1
0	100	1	1	484	20
0	1	10	1	1	1.7
0	1	100	1	1	84
0	1	1	$^1/_{10}$	12	1.7
0	1	1	$^1/_{100}$	832	141
0	1	10	$^1/_{10}$	12	17
0	10	1	$^1/_{10}$	598	110
0	10	10	1	14	129
0	10	10	$^1/_{10}$	604	345

[a] pMET and pTyr values normalized to the buildup observed at a ligand concentration of 0 nM. [b] The normalized values of 1 for k_{cat}, V_{max}, and pMET and pTyr represent the monomeric basal parameters and phosphorylation of c-MET and Tyr in the absence of ligand stimulation.

Nonstimulated monomeric c-MET exists in a tightly regulated inactive signaling state that is relatively insensitive to individual changes to its kinetic and thermodynamic parameters.

Synergistic Changes to c-MET Biochemical Properties. The k_{on} and k_{off} rates for the thermodynamic processes, the kinetic catalytic constants for autophosphorylation and effector phosphorylation, and rates of dephosphorylation of c-MET by phosphatases are the main biochemical parameters that differ between monomeric and dimeric c-MET. To better understand how oligomerization-induced changes to the thermodynamic, kinetic, and dephosphorylation properties of c-MET impact its activation, these properties were simultaneously varied for monomeric c-MET and the buildup of phosphorylated c-MET and pTyr was monitored (Table 3). These modeling studies were normalized to baseline simulations using monomeric and dimeric c-MET biochemical reaction parameters that were based on experimentally determined values (as described above). c-MET activation in the absence of extracellular ligand stimulation (and, hence, c-MET dimerization) was monitored by the level of accumulation of phosphorylated monomeric c-MET and pTyr. For comparison, normalized values of phosphorylated c-MET and pTyr in the presence of InlB are tabulated. As summarized in Table 3, c-MET and effector phosphorylation levels do not significantly change relative to the baseline simulation unless a biochemical parameter changed >100-fold relative to its default value. However, small changes in two or more kinetic properties have significant synergistic effects on c-MET's signaling competence. For example, decreasing the dephosphorylation rate (V_{26}) 10-fold and increasing autophosphorylation k_{cat} (k_{17}) and effector phosphorylation k_{cat} (k_{19} and k_{20}) 10-fold relative to the monomeric c-MET default parameters result in a buildup of phospho-

rylated c-MET and pTyr comparable to that observed at 20 nM InlB (Table 3). An order of magnitude change in the effector binding rate constants (k_2, k_3, k_6, and k_7) increases the basal levels of phosphorylated c-MET to ~0.5% of the total level of c-MET; however, these levels are several-fold lower than that generated in the presence of ligand. Thus, the generation of an activated c-MET state appears to be the result of synergistic effects between dynamic processes regulating receptor kinase activity (autophosphorylation and effector phosphorylation) and dephosphorylation.

If oligomerization synergistically modifies multiple biochemical parameters to regulate the phosphorylation state and hence the signaling activity of c-MET, will our model account for constitutive receptor activation? The TPR−MET complex is an excellent well-characterized example of a mutant c-MET protein that causes constitutive activation of c-MET in a manner independent of ligand stimulation and via receptor dimerization (*23*). The TPR−MET complex lacks mutations in its kinase domain but is able to dimerize and is tumorigenic due to the enhanced kinetic and thermodynamic properties associated with the dimeric species. Alternatively, it is clear that small synergistic changes in c-MET kinetic properties can result in a several-fold increased level of accumulation of phosphorylated c-MET and pTyr (Table 3). Interestingly, c-MET gain-of-function mutations (for example, D1228V, V1220I, Y1230H, Y1230C, D1228N, and V1220I) have been shown to lead to deregulated and prolonged kinase activity, which is critical to their transforming potential (*54*). The possible structural basis of ligand-independent activation via these mutations is discussed by Wang et al. (*55*), using the c-MET X-ray crystal structure. These structural changes may alter the biochemical properties of c-MET. The exact kinetic parameters of these mutants have not been measured directly, although it has been observed that some of these mutant forms of c-MET have high basal kinase activity in the absence of ligand (in their monomeric form) (*54*). The increased kinase activity of c-MET could directly impact the autophosphorylation (reaction 17) and effector phosphorylation (reactions 19 and 20) rates. If a c-MET point mutation increases the rates of autophosphorylation (reaction 17) and effector phosphorylation (reactions 19 and 20) 10-fold relative to that of the wild-type monomeric receptor, our model predicts that the unstimulated c-MET mutant would lead to an ~14-fold increase in the level of phosphorylated c-MET and an ~130-fold increase in the level of pTyr relative to that of the unstimulated wild-type receptor. The pTyr levels predicted from the point-mutated receptor are quantitatively similar to the amount of pTyr generated by the wild-type receptor following stimulation with 3 nM InlB (Table 3). c-MET point mutations that decrease the susceptibility of monomeric c-MET to dephosphorylation, and simultaneously increase the kinase autophosphorylation and effector phosphorylation catalytic efficiencies relative to that of wild-type c-MET, will result in a constitutively activate monomeric c-MET and phosphorylated c-MET and pTyr levels comparable to those observed for wild-type c-MET in response to saturating levels of ligand.

CONCLUSIONS

The use of computer modeling to predict cellular responses to RTK activation is being widely used (*1, 5, 45, 50, 56*).

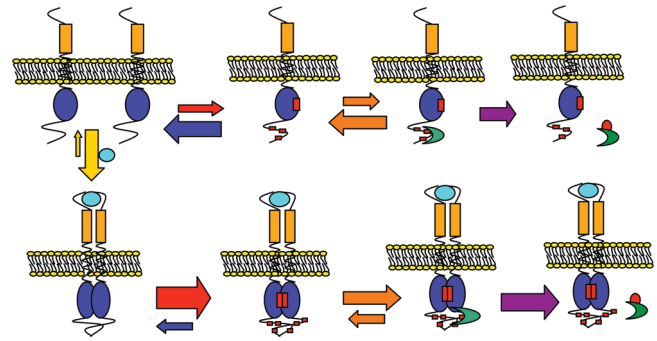

FIGURE 5: Model for c-MET activation. Shown is a model for c-MET activation based on experimental and modeling data. In the absence of an extracellular ligand stimulus, monomeric c-MET is localized to the cell surface and exists as a kinase active, but unphosphorylated, receptor. Monomeric c-MET phosphorylation and signaling are repressed due to decreased kinetic and thermodynamic properties of monomeric c-MET and its high susceptibility to dephosphorylation by PTPs. c-MET dimerization, in the presence of its cognate ligand, induces synergistic changes to the kinetic and thermodynamic properties of c-MET, which result in sustained c-MET autophosphorylation, effector recruitment and phosphorylation, and subsequent signaling.

Much of this work to date has focused on predicting downstream signal amplification and the flux through particular pathways in response to varying extracellular ligand stimulation. Until this work, an accurate model of c-MET (and by extension RTK) activation that takes into account the feed-forward loop that links autophosphorylation, dephosphorylation, and effector phosphorylation reactions has not been published.

The model presented here evaluates the relative importance of the main regulatory processes that work in concert to sharply switch between an inactive and active c-MET state. This model also addresses the importance of dimerization-mediated changes in c-MET kinetic, biochemical, and dephosphorylation properties for enabling activation specificity. Our model conclusively shows that ligand-stimulated c-MET is a highly competent signaling species and that its activation is sensitive to changes in its biochemical parameters. In contrast, unstimulated monomeric c-MET, although clearly an active kinase molecule, is incapable of existing in an activated (i.e., phosphorylated, signaling competent) state due to synergistic effects of the biochemical properties associated with the c-MET monomeric state. Thus, unstimulated monomeric c-MET is repressed in its ability to signal by virtue of its higher susceptibility to dephosphorylation and less efficient thermodynamic and kinetic properties relative to stimulated dimeric c-MET (Figure 5). If the biochemical properties of monomeric c-MET are synergistically altered, our model accurately predicts phosphorylated c-MET and pTyr could build to significant levels in the absence of extracellular ligand stimulation. Thus, the widespread use of the term "inactive" for monomeric unstimulated c-MET is not completely accurate and may be misleading. c-MET "activation" in the presence of an extracellular cognate ligand is more appropriately viewed as the accumulation of dimeric receptors that are capable of sustaining a phosphorylated state and signaling due to synergistic effects of the biochemical properties associated with that state. This activation mechanism, based on the experimental data and modeling predictions, is shown in Figure 5. This minimal activation model addresses the importance of oligomerization

in the activation process outlined in Figure 1a. The development of rigorous models that accurately describe c-MET (and related RTK) activation allows the critical determinants of receptor activation and signaling to be deconvoluted. Ultimately, these models could yield a more complete understanding of cell signaling and novel therapeutic approaches to treating disease involving aberrant receptor signaling. Our model highlights the three most important nodes critical for the inhibition in c-MET activation, namely, dimerization (i.e., ligand binding), c-MET kinase autophosphorylation, and effector substrate phosphorylation. Indeed, each of these nodes is under consideration for therapeutic intervention. Treatment strategies focusing on the antagonism of HGF binding include the development of anti-HGF antibodies and specific HGF-competitive antagonists (*57*−*60*). Furthermore, identification of small-molecule kinase inhibitors that lower the catalytic efficiency of c-MET continues to be a main focus of pharmaceutical companies for the treatment of cancers involving aberrant c-Met signaling (*61*−*63*).

ACKNOWLEDGMENT

We thank Dr. J. Papaconstantinou for the use of imaging equipment and software, M. Montes for excellent technical support, and Dr. G. Vande Woude for critical reading of our manuscript.

REFERENCES

1. Kholodenko, B. N., Demin, O. V., Moehren, G., and Hoek, J. B. (1999) Quantification of short term signaling by epidermal growth factor receptor. *J. Biol. Chem. 274*, 30169–30181.
2. Asthagiri, A. R., and Lauffenburger, D. A. (2000) Bioengineering models of cell signaling. *Annu. Rev. Biomed. Eng. 02*, 31–53.
3. Hubbard, S. R., and Till, J. H. (2000) Protein tyrosine kinase structure and function. *Annu. Rev. Biochem. 69*, 373–398.
4. Hunter, T. (1997) Oncoprotein networks. *Cell 88*, 333–346.
5. Moehren, G., Markevich, N., Demin, O., Kiyatkin, A., Goryanin, I., Hoek, J. B., and Kholodenko, B. N. (2002) Temperature dependence of the epidermal growth factor receptor signaling network can be accounted for by a kinetic model. *Biochemistry 41*, 306–320.
6. Pazin, M. J., and Williams, L. T. (1992) Triggering signaling cascades by receptor tyrosine kinases. *Trends Biochem. Sci. 17*, 374–378.
7. Schlessinger, J. (2000) Cell signaling by receptor tyrosine kinases. *Cell 103*, 211–225.
8. Schlessinger, J., and Ullrich, A. (1992) Growth factor signaling by receptor tyrosine kinases. *Neuron 9*, 383–391.
9. Hubbard, S. R., Mohammadi, M., and Schlessinger, J. (1998) Autoregulatory mechanisms of protein-tyrosine kinases. *J. Biol. Chem. 273*, 11987–11990.
10. Cobb, M. H., Sang, B. C., Gonzalez, R., Goldsmith, E., and Ellis, L. (1989) Autophosphorylation activates the soluble cytoplasmic domain of the insulin receptor in an intermolecular reaction. *J. Biol. Chem. 264*, 18701–18706.
11. Murray, B. W., Padrique, E. S., Pinko, C., and McTigue, M. A. (2001) Mechanistic effects of autophosphorylation on receptor tyrosine kinase catalysis: Enzymatic characterization of Tie2 and phospho-Tie2. *Biochemistry 40*, 10243–10253.
12. Parast, C. V., Mroczkowski, B., Pinko, C., Misialek, S., Khambatta, G., and Appelt, K. (1998) Characterization and kinetic mechanism of catalytic domain of human vascular endothelial growth factor receptor-2 tyrosine kinase (VEGFR2 TK), a key enzyme in angiogenesis. *Biochemistry 37*, 16788–16801.
13. Hubbard, S. R., Wei, L., Ellis, L., and Hendrickson, W. A. (1994) Crystal structure of the tyrosine kinase domain of the human insulin receptor. *Nature 372*, 746–754.
14. Hubbard, S. R. (1997) Crystal structure of the activated insulin receptor tyrosine kinase in complex with peptide substrate and ATP analog. *EMBO J. 16*, 5572–5581.
15. Rodrigues, G. A., and Park, M. (1994) Autophosphorylation modulates the kinase activity and oncogenic potential of the Met receptor tyrosine kinase. *Oncogene 9*, 2019–2027.
16. Kohanski, R. A. (1993) Insulin receptor autophosphorylation. I. Autophosphorylation kinetics of the native receptor and its cytoplasmic kinase domain. *Biochemistry 32*, 5766–5772.
17. Baer, K., Al-Hasani, H., Parvaresch, S., Corona, T., Rufer, A., Nolle, V., Bergschneider, E., and Klein, H. W. (2001) Dimerization-induced activation of soluble insulin/IGF-1 receptor kinases: An alternative mechanism of activation. *Biochemistry 40*, 14268–14278.
18. Baxter, R. M., Secrist, J. P., Vaillancourt, R. R., and Kazlauskas, A. (1998) Full activation of the platelet-derived growth factor β-receptor kinase involves multiple events. *J. Biol. Chem. 273*, 17050–17055.
19. Posner, B. I., Faure, R., Burgess, J. W., Bevan, A. P., Lachance, D., Zhang-Sun, G., Fantus, I. G., Ng, J. B., Hall, D. A., Lum, B. S., and Shaver, A. (1994) Peroxovanadium compounds. A new class of potent phosphotyrosine phosphatase inhibitors which are insulin mimetics. *J. Biol. Chem. 269*, 4596–4604.
20. Sheth, P. R., and Watowich, S. J. (2005) Oligomerization-induced differential dephosphorylation of c-MET receptor tyrosine kinase. *Biochemistry 44*, 10984–10993.
21. Hays, J. L., and Watowich, S. J. (2003) Oligomerization-induced modulation of TPR-MET tyrosine kinase activity. *J. Biol. Chem. 278*, 27456–27463.
22. Hays, J. L., and Watowich, S. J. (2004) Oligomerization-dependent changes in the thermodynamic properties of the TPR-MET receptor tyrosine kinase. *Biochemistry 43*, 10570–10578.
23. Rodrigues, G. A., and Park, M. (1993) Dimerization mediated through a leucine zipper activates the oncogenic potential of the met receptor tyrosine kinase. *Mol. Cell. Biol. 13*, 6711–6722.
24. Shimizu, A., Persson, C., Heldin, C. H., and Ostman, A. (2001) Ligand stimulation reduces platelet-derived growth factor β-receptor susceptibility to tyrosine dephosphorylation. *J. Biol. Chem. 276*, 27749–27752.
25. Ullrich, A., and Schlessinger, J. (1990) Signal transduction by receptors with tyrosine kinase activity. *Cell 61*, 203–212.
26. Birchmeier, C., Birchmeier, W., Gherardi, E., and Vande Woude, G. F. (2003) Met, metastasis, motility and more. *Nat. Rev. Mol. Cell Biol. 4*, 915–925.
27. Zhang, Y. W., Graveel, C., Shinomiya, N., and Vande Woude, G. F. (2004) Met decoys: Will cancer take the bait? *Cancer Cell 6*, 5–6.
28. Bottaro, D. B., Rubin, J. S., Faletto, D. L., Chan, A. M., Kmeicik, T. E., Vande Woude, G. F., and Aaronson, S. A. (1992) Identification of the hepatocyte growth factor receptor as the c-met proto-oncogene product. *Science 251*, 802–804.
29. Naldini, L., Vigna, E., Narsimhan, R. P., Gaudini, G., Zarnegar, R., Michalopoulos, G. K., and Comoglio, P. M. (1991) Hepatocyte growth factor (HGF) stimulates the tyrosine kinase activity of the receptor encoded by the proto-oncogene c-MET. *Oncogene 6*, 501–504.
30. Naldini, L., Weidner, M. K., Vigna, E., Gaudino, G., Bardelli, A., Ponzetto, C., Narsimhan, R. P., Hartmann, G., Zarnegar, R., and Michalopoulos, G. K. (1991) Scatter factor and hepatocyte growth factor are indistinguishable ligands for the MET receptor. *EMBO J. 10*, 2867–2878.
31. Hammond, D. E., Carter, S., McCullough, J., Urbe, S., Vande Woude, G. F., and Clague, M. E. (2003) Endosomal dynamics of met determines signaling output. *Mol. Cell. Biol. 14*, 1346–1354.
32. Li, N., Xiang, G. S., Dokainish, H., Ireton, K., and Elferink, L. A. (2005) The *Listeria* protein InlB mimics hepatocyte growth factor-induced receptor trafficking. *Traffic 6*, 459–473.
33. Naldini, L., Vigna, E., Ferracini, R., Longati, P., Gandino, L., Prat, M., and Comoglio, P. M. (1991) The tyrosine kinase encoded by the MET proto-oncogene is activated by autophosphorylation. *Mol. Cell. Biol. 11*, 1793–1803.
34. Bertics, P. J., Weber, W., Cochet, C., and Gill, G. N. (1985) Regulation of the epidermal growth factor receptor by phosphorylation. *J. Cell. Biochem. 29*, 195–208.
35. Biswas, R., Basu, M., Sen-Majumdar, A., and Das, M. (1985) Intrapeptide autophosphorylation of the epidermal growth factor receptor: Regulation of kinase catalytic function by receptor dimerization. *Biochemistry 24*, 3795–3802.
36. Villalba, M., Wente, S. R., Russell, D. S., Ahn, J. C., Reichelderfer, C. F., and Rosen, O. M. (1989) Another version of the human receptor kinase domain: Expression, purification and characterization. *Proc. Natl. Acad. Sci. U.S.A. 86*, 7848–7852.

37. Weber, W., Bertics, P. J., and Gill, G. N. (1984) Immunoaffinity purification of the epidermal growth factor receptor. Stoichiometry of binding and kinetics of self-phosphorylation. *J. Biol. Chem. 259*, 14631–14636.
38. Treadway, J. L., Morrison, B. D., Soos, M. A., Siddle, K., Olefsky, J., Ullrich, A., McClain, D. A., and Pessin, J. E. (1991) Transdominant inhibition of tyrosine kinase activity in mutant insulin/insulin-like growth factor I hybrid receptors. *Proc. Natl. Acad. Sci. U.S.A. 88*, 214–218.
39. Sherrill, J. M. (1997) Self-phosphorylation of epidermal growth factor receptor is an intermolecular reaction. *Biochemistry 36*, 12890–12896.
40. Yarden, Y., and Schlessinger, J. (1987) Epidermal growth factor induces rapid, reversible aggregation of the purified epidermal growth factor receptor. *Biochemistry 26*, 1443–1451.
41. Iwasaki, Y., Nishiyama, H., Suzuki, K., and Koizumi, S. (1997) Sequential cis/trans autophosphorylation in TrkB tyrosine kinase. *Biochemistry 36*, 2694–2700.
42. Kohanski, R. A. (1993) Insulin receptor autophosphorylation. I. Autophosphorylation kinetics of the native receptor and its cytoplasmic kinase domain. *Biochemistry 32*, 5766–5772.
43. Furge, K. A., Zhang, Y. W., and Vande Woude, G. F. (2000) Met receptor tyrosine kinase: Enhanced signaling through adapter proteins. *Oncogene 19*, 5582–5589.
44. Pelicci, G., Giordano, S., Zhen, Z., Salcini, A. E., Lanfrancone, L., Bardelli, A., Panayotou, G., Waterfield, M. D., Ponzetto, C., Pelicci, P. G., and Comoglio, P. M. (1995) The motogenic and mitogenic responses to HGF are amplified by the Shc adapter protein. *Oncogene 10*, 1631–1638.
45. Posner, I., Engel, M., and Levitzki, A. (1992) Kinetic model of the epidermal growth factor (EGF) receptor tyrosine kinase and a possible mechanism of its activation by EGF. *J. Biol. Chem. 267*, 20638–20647.
46. Ireton, K., Payrastre, B., and Cossart, P. (1999) The *Listeria monocytogenes* protein InlB is an agonist of mammalian phosphoinositide 3-kinase. *J. Biol. Chem. 274*, 17025–17032.
47. Li, N., Lorinczi, M., Ireton, K., and Elferink, L. A. (2007) Specific Grb2-mediated interactions regulate clathrin-dependent endocytosis of the cMet-tyrosine kinase. *J. Biol. Chem. 282*, 16764–16775.
48. Shen, Y., Naujokas, M. A., Park, M., and Ireton, K. (2000) InlB-dependent internalization of *Listeria* is mediated by the Met receptor tyrosine kinase. *Cell 103*, 501–510.
49. Machner, M. P., Frese, S., Schubert, W., Orian-Rousseau, V., Gherardi, E., Wehland, J., Niemann, H. H., and Heinz, D. W. (2003) Aromatic amino acids at the surface of InlB are essential for host cell invasion by *Listeria monocytogenes*. *Mol. Microbiol. 48*, 1525–1536.
50. Wiley, H. S., Shvartsman, S. Y., and Lauffenburger, D. A. (2003) Computational modeling of the EGF-receptor system: A paradigm for systems biology. *Trends Cell Biol. 13*, 43–50.
51. Offterdinger, M., Georget, V., Girod, A., and Bastiaens, P. I. H. (2004) Imaging phosphorylation dynamics of the epidermal growth factor receptor. *J. Biol. Chem. 279*, 36972–36981.
52. Seveau, S., Bierne, H., Giroux, S., Prevost, M.-C., and Cossart, P. (2004) Role of lipid rafts in E-cadherin-and HGF-R/Met-mediated entry in *Listeria moncytogenes* into host cells. *J. Cell Biol. 166*, 743–753.
53. Jeffers, M., Schmidt, L., Nakaigawa, N., Webb, C. P., Weirich, G., Kishida, T., Zbar, B., and Vande Woude, G. F. (1997) Activating mutations for the met tyrosine kinase receptor in human cancer. *Proc. Natl. Acad. Sci. U.S.A. 94*, 11445–11450.
54. Danilkovitch-Miagkova, A., and Zbar, B. (2002) Dysregulation of Met receptor tyrosine kinase activity in invasive tumors. *J. Clin. Invest. 109*, 863–867.
55. Wang, W., Marimuthu, A., Tsai, J., Kumar, A., Krupka, H. I., Zhang, C., Powell, B., Suzuki, Y., Nguyen, H., Tabrizizad, M., Luu, C., and West, B. L. (2006) Structural characterization of autoinhibited c-MET kinase produced by coexpression in bacteria with phosphatase. *Proc. Natl. Acad. Sci. U.S.A. 103*, 3563–3568.
56. Sachs, K., Gifford, D., Jaakkola, T., Sorger, P., and Lauffenburger, D. A. (2002) Bayesian network approach to cell signaling pathway modeling. *Sci. STKE 148*, PE38.
57. Boccaccio, C., Ando, M., Tamagnone, L., Bardelli, A., Michieli, P., Battistini, C., and Comoglio, P. M. (1998) Induction of epithelial tubules by growth factor HGF depends on the STAT pathway. *Nature 391*, 285–288.
58. Cao, B., Su, Y., Oskarsson, M., Zhao, P., Kort, E. J., Fisher, R. J., Wang, L.-M., and Vande Woude, G. F. (2001) Neutralizing monoclonal antibodies to hepatocyte growth factor/scatter factor (HGF/SF) display antitumor activity in animal models. *Proc. Natl. Acad. Sci. U.S.A. 98*, 7443–7448.
59. Mazzone, K., Basilico, C., Cavassa, S., Pennacchietti, S., Risio, M., Naldini, L., Comoglio, P. M., and Michieli, P. (2004) An uncleavable form of pro-scatter factor suppresses tumor growth and dissemination in mice. *J. Clin. Invest. 114*, 1418–1432.
60. Ogiso, H., Ishitani, R., Nureki, O., Fukai, S., Yamanaka, M., Kim, J. H., Saito, K., Sakamoto, A., Inoue, M., Shirouzu, M., and Yokoyama, S. (2002) Crystal structure of the complex of human epidermal growth factor and receptor extracellular domains. *Cell 110*, 775–787.
61. Christensen, J. G., Burrows, J., and Salgia, R. (2005) c-MET as a target for human cancer and characterization of inhibitors for therapeutic intervention. *Cancer Lett. 225*, 1–26.
62. Christensen, J. G., Schreck, R., Burrows, J., Kuruganti, P., Chan, E., Le, P., Chen, J., Wang, X., Ruslim, L., Blake, R., Lipson, K. E., Ramphal, J., Do, S., Cui, J. J., Cherrington, J. M., and Mendel, D. M. (2003) A selective small molecule inhibitor of c-MET kinase inhibits c-MET dependent phenotype in vitro and exhibits cytoreductive antitumor activity in vivo. *Cancer Res. 63*, 7345–7355.
63. Smolen, G. A., Sordella, R., Muir, B., Mohapatra, G., Barmettler, A., Archibald, H., Kim, W. J., Okimoto, R. A., Bell, D. W., Sgroi, D. C., Christensen, J. G., Settleman, J., and Haber, D. A. (2006) Amplification of MET may identify a subset of cancers with extreme sensitivity to the selective tyrosine kinase inhibitor PHA-665752. *Proc. Natl. Acad. Sci. U.S.A. 103*, 2216–2221.

BI701892F